

Phase transition in ZnS nanoparticles: electrical, thermal, structural, optical, morphological, antibacterial and photocatalytic properties

M. M. Rose^a, R. S. Christy^b, T. A. Benitta^b, J. T. T. Kumaran^c, M. R. Bindhu^{d,*}

^aResearch scholar (Reg.No:18123112132030), Department of Physics and Research Centre, Nesamony Memorial Christian College, Marthandam, Affiliated to Manonmaniam Sundaranar University, Abishekapatti, Tirunelveli-629165, TamilNadu, India

^bDepartment of Physics and Research Centre, Nesamony Memorial Christian College, Marthandam-629301, TamilNadu, India

^cDepartment of Physics and Research Centre, Malankara Catholic College, Mariagiri, Kaliyakkavilai, TamilNadu, India

^dDepartment of Physics, Sree Devi Kumari Women's College, Kuzhithurai-629163, Tamil Nadu, India

Zinc Sulphide nanoparticles (ZnS-NPs) are synthesized by microwave assisted chemical precipitation method. The as-synthesized nanoparticles are identified by X ray diffraction and electrical studies to examine the structural transition. The HT-XRD at 100^oC (373 K) and 200^oC (473 K) of ZnS-NPs also confirms structural transition of cubic to hexagonal phase. Thermal properties of the ZnS sample is also studied using thermo gravimetric-differential thermal analysis (TG-DTA). From D.C. electrical resistance, a discontinuity occurs in the temperature resistance curve of the ZnS-NPs due to phase transition around 450 K. The energy dispersed x-ray analysis and Raman spectra of the ZnS-NPs confirm the presence of zinc and sulphur. The optical studies of the prepared ZnS-NPs are confirmed by its UV-vis and PL spectra. The TEM image of cubic ZnS-NPs reveals the well distribution of spherical shaped particles with mean size of 12.52 nm with standard deviation of 9.326 nm. According to the photocatalytic results of ZnS-NPs for the degradation of methylene blue (MB) have the highest degradation efficiency of 93.24% under UV irradiation within 80 min. Antibacterial effects of ZnS-NPs nanoparticles against some pathogens, like gram-negative, gram-positive, *E. coli* (*Escherichia coli*), *S. aureus* (*Staphylococcus aureus*) bacteria.

(Received August 23, 2022; Accepted November 24, 2022)

Keywords: Zinc sulphide, Chemical precipitation, Phase transition, Hexagonal, Raman, Photodegradation

1. Introduction

Fabrication industries have led to crucial calamity in supplying clean water pertaining to the whole world [1]. The water pollution is mainly caused by organic dyes, mechanisms to prevent this are still in question [2]. Nowadays, the organic dye removal from industrial waste water utilizing photocatalysis has gained much research interest [3-8]. Different semiconductor photocatalysts have been taken into consideration in this regard because of their excellent efficacy in degrading water pollutants without producing any harmful by products. Recently, in photocatalysis field, semiconductor sulphides have demonstrated substantial significance. According to this theory, ZnS-NPs with a broad band gap of 3.6 eV—3.8 eV, have appeared its

* Corresponding authors: bindhufm@gmail.com
<https://doi.org/10.15251/CL.2022.1911.855>

potential as an active photocatalyst for the purification of water by degradation of organic pollutants, CO₂ reduction and water splitting [9-13]. These heterogeneous photocatalysts have the unique property of using light to produce electron-hole pairs under UV-light irradiation in the medium. Only a small number of generated electron-hole pairs are able to spread out to its stage to carry out the chemical reaction with substrates or atmospheric water. As the conduction band of the ZnS catalyst is situated upper than that of the prominent photocatalyst (TiO₂), an extremely negative lessening potential is predicted to endorse its photo-catalytic activity superior to TiO₂. However, the tiny lattice-energy of ZnS-NPs show the way to develop into its bulk counterparts, which leads to organic pollutants degradation [14]. ZnS nanostructure is a well-researched material that is employed as a photocatalyst for organic pollutants removal, such as Methylene Blue (MB). Chauhan et al. have reported about the photocatalytic response of ZnS and observed that ZnS degraded about 66% of MB in 300 min of irradiation [15]. Soltani et al., have studied the photocatalytic deterioration of MB under visible light utilizing PVP-capped ZnS nanoparticles [16]. Guo et al., have investigated the photocatalytic reactivity presented by PVDF-ZnS pellets is the major removal methods with MB mixture in wastewater treatment [17]. Sharma et al., have reported the photocatalytic degradation of MB subject to UV-visible light utilizing ZnS-NPs nanoparticles [18]. Zinc Sulphide nanoparticles display a wide-spectrum biocide which is used to destroy, render harmless, or have some kind of controlling effect on a harmful organism towards multiple viruses, bacteria, and fungi [19, 20]. The antibacterial activity of prepared ZnS nanoparticles are examined against *E. Coli*, and *S. aureus*.

Here, to attain high photo-catalytic activity of the ZnS-NPs, the particle morphology controlling, size with phase transition are regarded as one of the significant measure [19,20]. Small nano sized ZnS-NPs established very active photo-catalyst owing to its higher surface area to volume (SA:V) ratio [20,21,22]. It is also reported as the cubic phase is highly active towards the photocatalytic applications than the hexagonal phase [23]. Hence, there is still a necessitate to prepare a low-cost and simple method for cubic phase ZnS-NPs with small size (high SA:V ratio) and well dispersed spherical shaped particles.

The demand for new nanomaterials with superior anti-bacterial actions is on go up with the emergence of drug resistance bacterial strains, and the antibacterial applications of nano sized sulphides are mostly examined [24]. The electrical, optical and morphological characteristics as well as the synthesis method ZnS-NPs influence the anti-bacterial activity of ZnS-NPs [25]. Organic anti-bacterial agents and antibiotics have several drawbacks such as toxicity to human beings and animals, so an attention in inorganic disinfectants such as metal oxides/sulphides NPs is on get higher among research groups [26]. The development of advanced biocompatible nano sized semiconductor sulphides with antibacterial activities could be potential for environmental applications such as in medicine, water disinfection, food packaging and textile industry [27,28].

ZnS-NPs have successfully synthesized by solvothermal [29], hydrothermal [30], sol-gel [31], sonochemical [32], microwave irradiation [33] and microemulsion [34]. The microwave-assisted synthesis modes contain few merits involving rapid and uniform heating, process of energy savings, lesser preparation time, lesser processing cost, smaller narrow particle size distribution, higher purity over other methods. Qadri et al., have reported about the transformation from the cubic ZnS to the hexagonal structure at low temperatures [35]. Cuizhuo Yang et al., observed phase transition through sphalerite structure to wurtzite structure on ZnS-NPs under 1 GPa pressure [36]. Arup Kanti Kole et al., have studied co-precipitation method base the phase transition in ZnS-NPs synthesized [37]. Yiyu Li et al. investigated the phase transition behaviour of ZnS ceramics [38].

In this study, synthesized ZnS-NPs by microwave assisted chemical precipitation method with the purpose to reveal its function as a photocatalytic agent, so it is employed for the water purification applications. Structural transitions were studied using DC electrical measurements and HT-XRD. The TGA and DTA results were studied. The UV, PL, Raman spectra of ZnS sample are analyzed. The photodegradation of organic dye through ZnS-NPs investigated under UV light irradiation.

2. Experimental techniques

2.1 Synthesis of ZnS-NPs through microwave assisted chemical precipitation approach

Zinc acetate along sodium sulphide are considered into initiating materials on 1:2 molar ratio for synthesised ZnS-NPs. Zinc acetate solution is introduced by dissolving 10.97 g of zinc acetate in 50 ml distilled water. Where, 7.8 g sodium sulphide dissolves in 50 ml distilled water. Under effectual stirring, the sodium sulphide solution is included to zinc acetate solution in drops. After 3 hours of constant stirring, a white-colored solution is produced, it remains undisturbed per day. The precipitates are separated out severally and cleaned using deionized water. The solution is put through 800 W microwave irradiations at twenty minutes. The nanoparticles are acquired then refrigerated with room temperature. The annealed of nanoparticles for 3 hrs at 100°C to get phase pure ZnS-NPs. The collected ZnS-NPs were used for different characterization.

2.2. Instrumentation

X-ray diffraction (XRD) patterns of ZnS-NPs are take down on a Cu K α radiation $\lambda = 1.54 \text{ \AA}$ along powder X-ray diffractometer including 2θ ranges of angles $10^\circ - 80^\circ$. ZnS-NPs formation is confirmed through TEM micrographs collected via (JEOL 2000 FX 11). The element compositions are confirmed using energy dispersive X-ray analysis (EDAX) set up hooked with scanning electron microscope (TESCAN VEGA3 SBH Scanning Electron Microscope). A set of nano particles (pellet) is acquired by 10 tones/cm² higher pressure Four-probe approach is used to measure the samples' resistance in pellet form. The thermogravimetric study (TGA) and differential thermal analysis (DTA) were carryout using PerkinElmer STA 8000 on the sample at a heating rate of 10 °C/min in the temperature range 40–1300 °C. On a UV-visible spectrometer, the optical absorption spectrum of the synthesized nanoparticles is captured in the 200-900 nm region. In Varian Cary Eclipse Photoluminescence spectrophotometer, photoluminescence measurements are activated within 300-650 nm range. ZnS-NPs Raman spectrum records by peak Seeker Raman spectrometer. The photocatalytic properties of the ZnS-NPs are characterized by UV-VIS spectroscopy utilizing Shimadzu UV-1619PC spectrophotometer at 200-800 nm range.

3. Results with discussion

3.1. Structural studies

Room temperature X-ray Diffraction (RT-XRD) pattern of prepared ZnS-NPs is depicted in Fig.1. The XRD traces of the prepared ZnS-NPs shows that three peaks at 28.74° , 48.13° , 56.63° , 70.72° and 77.66° for the Bragg planes (111), (220), (311), (400) and (331) respectively and it indicates that the prepared NPs have Face centered cubic structure along space group F43m. Any peaks of crystalline impurities haven't been found out. The lattice parameters and cell volume of the prepared nanoparticles calculated as $a=b=c=5.329 \text{ \AA}$ and $V= 151.33 \text{ \AA}^3$ which agrees with the reported value $a=5.345 \text{ \AA}$ and $V=152.70 \text{ \AA}^3$ (JCPDS: 80-0020) [39]. It can be observed that the broadening of peaks signifies its small crystalline sizes [40]. In fact, the wideness of a specific phase of nanomaterial and its crystallite size are directly proportional to each other. The particle size was calculated using Debye Scherer formula [41] and it is found to be 9.62 nm.

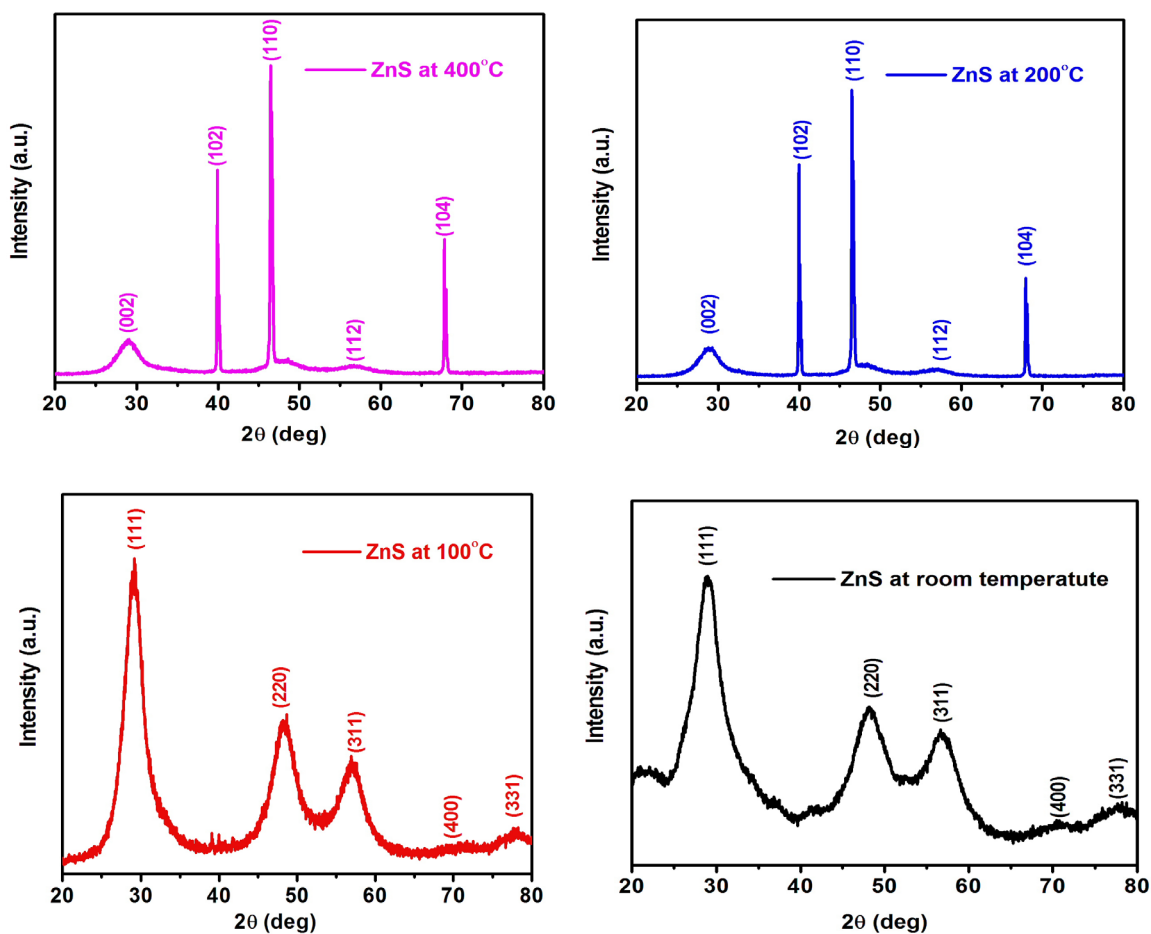


Fig. 1. Indexed RT-XRD and HT-XRD pattern of ZnS-NPs by microwave assisted chemical precipitation method at room temperature, 100°C (373K), 200°C (473K) and 400°C (673K).

The high temperature X-ray Diffraction (HT-XRD) pattern of the prepared ZnS-NPs is taken to establish its phase transition is shown in Fig. 1. Here, the HT-XRD pattern of ZnS-NPs at 373K (100°C) is represented. There is no variation in the XRD pattern recorded at room temperature and 373K, and the obtained results agree well with the standard data, JCPDS: 80-0020. The particle size indicates 15.05 nm. Fig 1 represents HT-XRD pattern of ZnS-NPs recorded at 473K (200°C) and can be indexed to (002), (102), (110), (112) and (104) planes at 28.88°, 40.07°, 46.33°, 56.62° and 67.60° respectively (JCPDS:80-0007). It indicates that the prepared NPs have primitive hexagonal structure with space group P63mc. The lattice parameters of the prepared nanoparticles calculated as $a=b=3.9\text{Å}$ and $c=6.14\text{Å}$ which agrees with the reported value $a=b=3.777\text{Å}$ and $c=6.188\text{Å}$ (JCPDS: 80-0007). The particle size was also calculated to be 64.41 nm. This clearly indicates that there is a transition from cubic to hexagonal at a transition temperature about 473K (200°C). The change over of transition from cubic to hexagonal is a nucleation and growth process in terms of temperature, morphology, also the reagents used in the synthesis.

To study if there is any further transition, HT-XRD pattern was obtained at 673K (400°C) (Fig.1). It shows similar structure and also peaks are at the same position. Since the HT-XRD patterns obtained at 473 K (200°C) and 673 K (400°C) are similar, there may be either no transition in between or after transition it may returned again to same structure similar to the transition reported in CdS nanoparticles [42]. Based on the obtained XRD results, the sharpening of XRD peaks and increasing particle size were obtained with the phase transition from cubic (room temperature) to hexagonal (673 K).

3.2. Electrical studies

At 300 K—500 K temperature range, the D.C electrical resistances of pellet-shaped ZnS-NPs synthesized utilizing microwave assisted chemical precipitation method. The curve of resistance variation with temperature of ZnS-NPs is represented in Fig.2. The curve contains two regions. First region is from 300 K to 450 K and next one is above 450 K. The temperature resistance curve remains constant upto 450 K. In this region the resistance of the sample is of the order of 10^9 ohm and the sample behaves as an insulator. Similar electrical behavior at room temperature and 373 K, and the same cubic structure of the XRD patterns obtained at the corresponding temperatures reveals that unless the electrical behavior changes structure remains the same. Above 450 K the resistance decreases with increase in temperature showing semiconducting behavior. This change in electrical behavior around 450 K (Fig.2) is also seen in the XRD patterns obtained above and below 450 K.

To study if there is any shift in transition temperature on further heating the experiment was repeated again and again after cooling it to room temperature and is shown in Fig.2b. Even though there is slight change in the transition temperature when the time gap between the two trials is small, but after giving suitable time gap between two trials the graph obtained was similar to the first trial. The insulating property of the sample in the region 300 K to 450 K is not affected by repeated heating and cooling unlike hexagonal CdS [42]. Hence ZnS-NPs can be used as a very good insulator in the region 300 K to 450 K. As the resistance decreases rapidly with temperature above 450 K it can be also used as a temperature sensor.

Thus, the phase transition from cubic to hexagonal is determined by electrical studies of ZnS-NPs then the attained results are subject to XRD results. Hence, the structure varies for different electrical behavior. This clearly indicates that the structural transition can be studied from temperature resistance measurements. The similar transition was already reported by varying annealing temperature and pressure [37, 39].

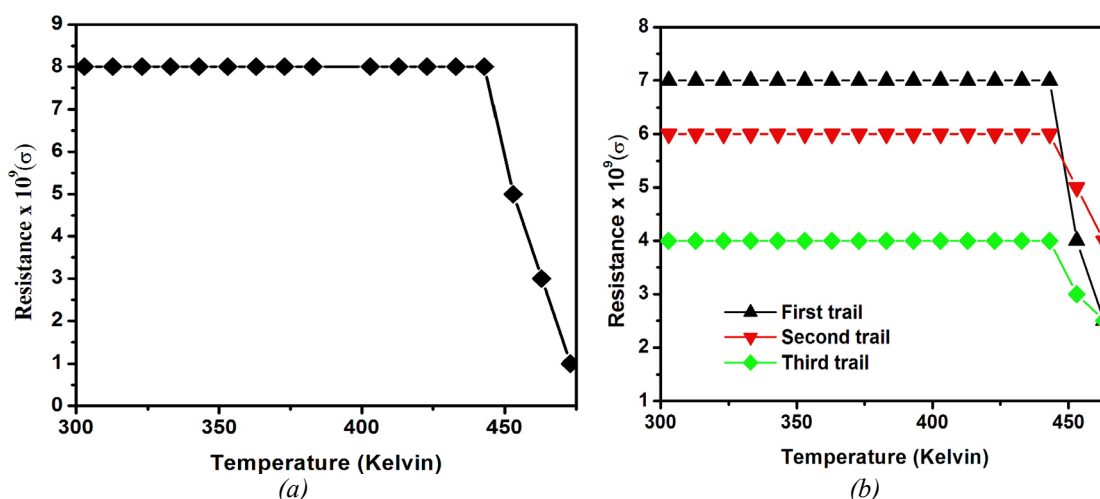


Fig. 2. Variation (a) and different trials (b) of resistance with temperature of ZnS-NPs synthesized.

3.3. Thermal studies

The thermal behavior of ZnS-NPs has been explored by thermo gravimetric analysis (TGA) together with differential thermal analysis (DTA). ZnS-NPs is analyzed by TGA in order to check their relative stabilities. The TGA thermogram of the ZnS-NPs is presented in Fig. 3 (a). The TGA graph shows the major weight loss start from 200°C (473 K) and weight loss is 30%. This may be due to the thermal degradation of the unstable constituents in the sample and the evaporation of residual moisture or solvent absorbed to the surface or inner of the samples. From 300°C – 800°C there is no weight loss. Senapati U. S et al discussed the thermal stability of the sample upto 200°C [43]. This indicates that the sample is thermally stable upto 200°C (473 K),

which is probably due to interaction between the particles. The stability of the prepared nanoparticles is also confirmed by the D.C. electrical studies.

Less or more heat required to flow for maintaining both at the same temperature when the sample goes through a phase transition. Depending on whether the process is exothermic or endothermic, either less or more heat must be transferred to the sample. The first endothermic peak and exothermic peak (Fig.3 (b)) in the ZnS-NPs is around 200°C. This confirms the structural phase transition from cubic to hexagonal; the attained results are confirmed with XRD and electrical studies.

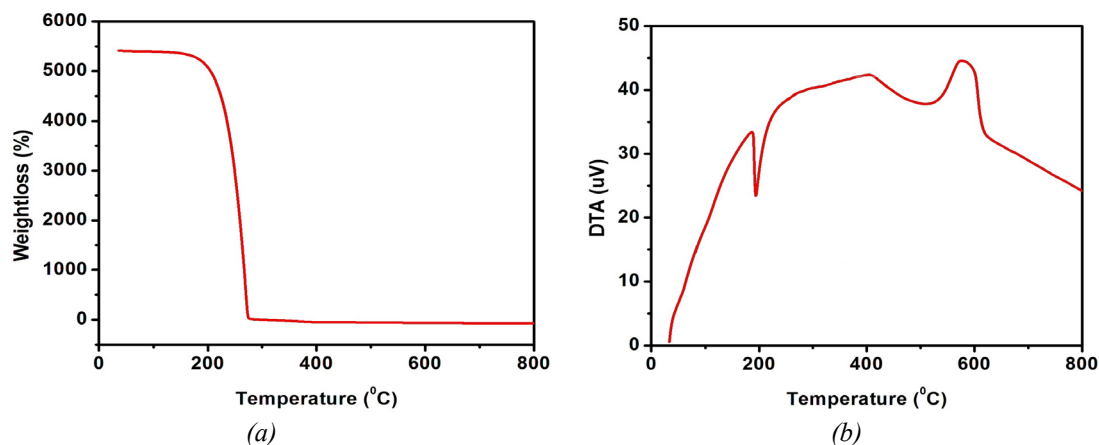


Fig. 3. (a) TGA and (b) DTA curve of ZnS-NPs.

3.3. Optical studies

UV-v is absorption spectrum of ZnS-NPs is implicated in Fig. 4 (a). Here, the absorption band is around 350 nm [44]. Because of every wavelength under 350 nm, it can be used as an optical filter. Band gap energy is obtained by plotting Tauc's plot [45]. Using the Tauc's relation, the absorption co-efficient for direct band gap indicates $\alpha = A (h\nu - E_g)^n / h\nu$ here, A is a constant α is absorption co efficient, E_g is band gap energy, $h\nu$ implies incident photon energy $n=1/2$ to straight permitted transition. The band gap energy is acquired by extrapolating the straight line portions of $h\nu$ verses $(\alpha h\nu)^2$ (Fig.4 (b)). The direct band gap value is 3.72 eV which concurs with reported value [46]. The ZnS-NPs optical band edge is shifted towards lower wavelength side (band gap of bulk ZnS of 3.68 eV)[47] on account of quantum size effect, also initiates from the e^-/h^+ confinement in a small sized volume in its electronic-structure, there is higher value of band gap energy happened. Due to its wide band gap it can be used as a photosensitive material for photon detection in the UV range.

Fig.4(c) shows the PL emission spectrum of ZnS-NPs including 320 nm excitation wavelengths. There is a high intense peak obtained around 390 nm and also peaks are observed at 363,411,438 and 490 nm which is attributed to ZnS-NPs. Generally, the emission at the visible region attributes to the acceptor transition band whereas the deep level emission is accredited to the impurities and structural defects the in the reaction medium [48]. The prepared ZnS-NPs illustrate the long lifetime of photo-generated charges and it can be attributed to the inhibited recombination of charges or the effectual separation of electrons and holes, which might enhance the photocatalysis performance of ZnS-NPs.

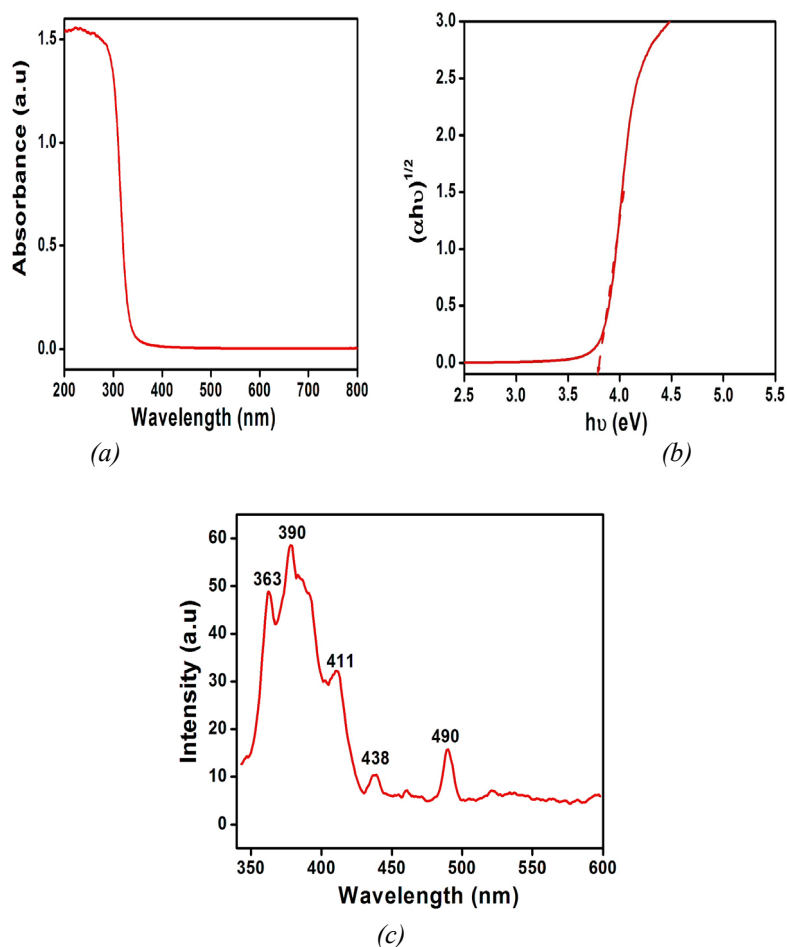


Fig. 4. Optical absorption, (b) Tauc's plot and (c) emission spectra of ZnS-NPs.

3.4. Raman studies

Fig 5 depicts the Raman spectrum of ZnS-NPs. The peaks observe at 290cm^{-1} , 340cm^{-1} and 411cm^{-1} . The peaks around 275cm^{-1} represents transverse optical (TO) phonon mode as well as peak around 340cm^{-1} is assigned to longitudinal optical mode (LO)[49-50]. The peaks in between 275cm^{-1} and 340cm^{-1} were already reported by previous works and this is the characteristic of the ZnS-NPs [51-52]. The shifts of the TO and LO modes to lower wave number observed in the ZnS- NPs can be credited to a larger surface area : volume (SA:V) ratio and smaller particle size when compared with that of the ZnS reported by previous works [53-54]. Here with smaller particle size and larger SA:V ratio of the prepared ZnS-NPs, the contribution of surface-scattering to the Raman signal is more than that of volume-scattering. In addition, the purity phase of the prepared ZnS-NPs is confirmed by the absence of extra Raman modes.

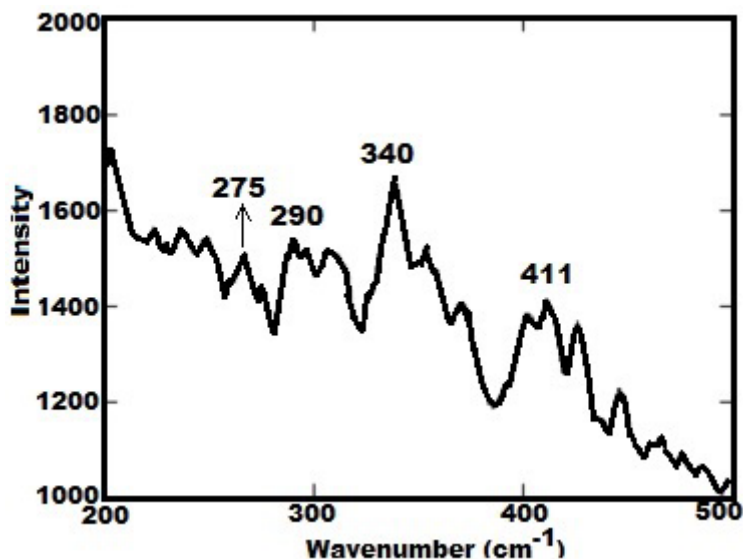


Fig. 5. Raman spectrum of ZnS nanoparticles.

3.5. Morphological studies

The TEM image of cubic ZnS-NPs (Fig.6a-d)) in four different scales 100, 50, 20 and 10 nm, which reveals the well distribution of spherical shaped ZnS-NPs with mean size of 12.52 nm lies between 6.56 nm and 56.12 nm with standard deviation of 9.326 nm. The spherical particles with good dispersion get more attention because of its capability to create the photonic-crystal assembly (a periodic optical nanostructure) [55]. It can affect the motion of photons and it confines light that likely progresses the photocatalytic efficiency [56]. The median, mode and mean values of the distribution of particle size are different. Mean value (124.067) is larger than that of mode (116.032) and median (122.265) which indicates the occurrence of smaller sized particles in larger number, in assessment to larger sized nanoparticles, because of the control in size of spherical particles. In Fig. 6 (c), a tiny section marked by a square is magnified. Fig.6 (d) shows 0.302 nm lattice space with respect to the plane (111) of face centered cubic plane. Fig. 6(e) displays the crystalline nature of cubic ZnS-NPs which is recognized through the chosen area electron diffraction pattern along brightest spots depends on Bragg planes ((111), (220), (311), (400) and (331)). Fig.6f reveals the EDAX image of ZnS-NPs. The purity of ZnS nanoparticles were also confirmed by EDAX analysis. It confirms the existence of zinc and sulphur in proper ratio. The composition of present investigated ZnS sample shows 46.45 % and 53.55 % of Zn and S respectively.

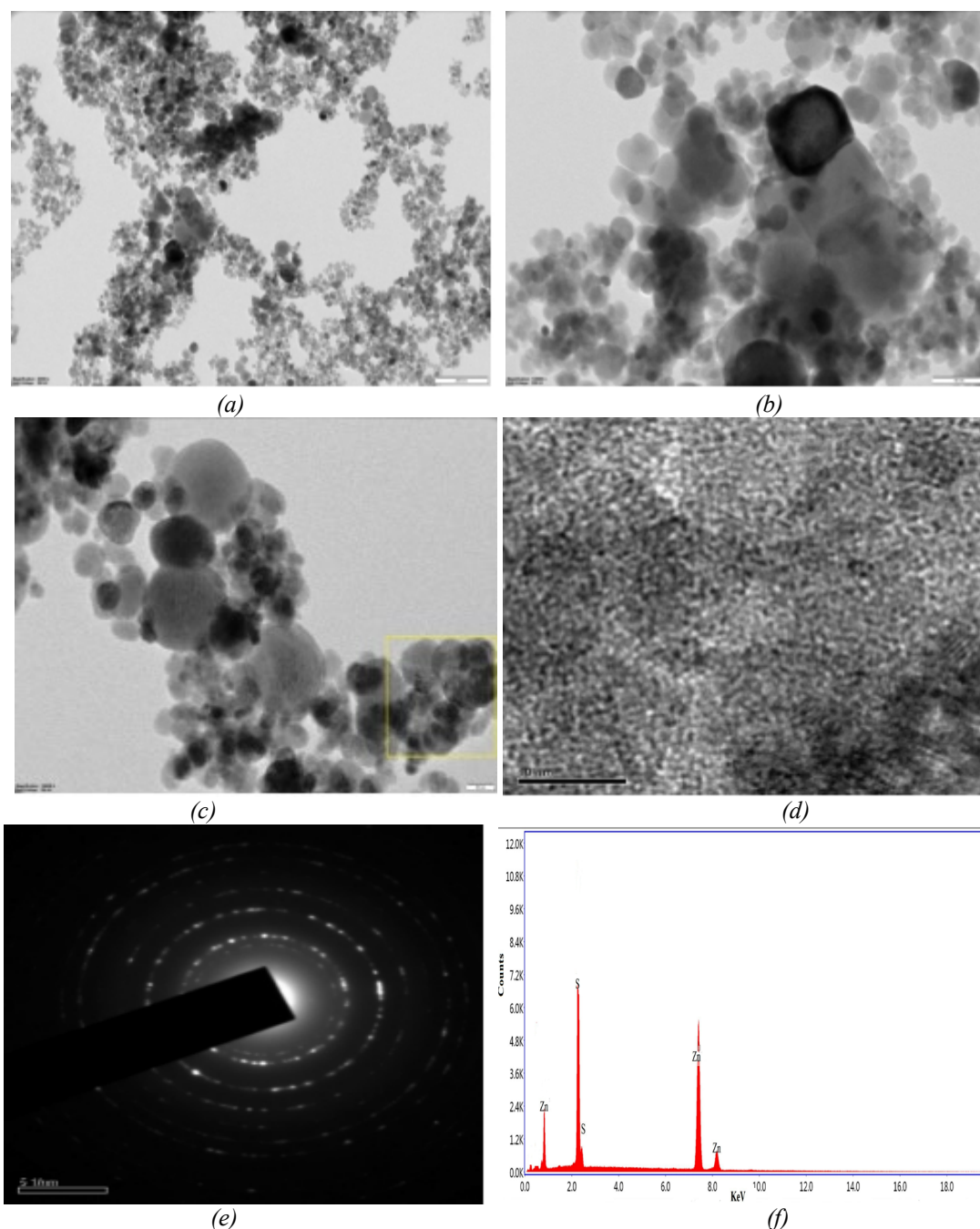


Fig. 6. (a-d) TEM image of cubic ZnS-NPs in four different scales 100, 50, 20 and 10 nm; (e) crystalline nature of cubic ZnS-NPs which is recognized through the selected area electron diffraction pattern and (f) EDAX image of ZnS-NPs.

3.6. Photocatalytic studies of ZnS-NPs

The unaffordability of pure drinking water is the main cause of most diseases. Industrial dyes are the major reason for polluting drinking water. Methylene blue (MB) is a noxious, dangerous, and non-corroding and make severe diseases. So, there is a requirement to develop an environmental friendly, systematic technology for eradicating methylene blue from water. A sophisticated oxidation method that is broadly utilized to dyes removal is Photodegradation. With the potential to lower the cost of refining, it can change total mineralization of dye as simple and nontoxic species. In this study, the ZnS-NPs photocatalytic studies are evaluated by methylene blue degradation under UV irradiation because it has high light absorbing properties (98% of

transmitted light absorbed) and applications as a redox indicator in analytical chemistry. When MB dye mixed ZnS-NPs absorbs light energy ($h\nu$) exceeded/equal to the band gap of ZnS-NPs, it causes excitation of valence-band electrons (e^- s) to the conduction-band. At the same time, it produces an electron vacancy (positive charged hole) (h^+) on valence-band. Then e^- s and h^+ s separation taken place by the excitation. These e^- s and h^+ s drifted towards the surface of the material and react with adsorbed oxygen and hydroxide in reaction medium. And further produced free radicals such as OH^\bullet , $O_2^{\bullet-}$, HO_2^\bullet and H_2O_2 in the reaction medium. These active oxygen species can direct to the complete/partial mineralization of MB.

After exposing the solution with UV irradiation, the absorption spectrum MB solution with ZnS-NPs measured at various time intervals. If the time interval rises from 0 to 100 mins, the absorption spectra intensity will decrease. Fig 7 (a) signifies UV-Vis absorbance spectra of MB degradation by ZnS-NPs. Here, the absorption peaks intensity is diminished owing to the MB degradation. The MB degradation solution with ZnS nanoparticles under UV irradiation is linear and uniform. This clearly indicates that ZnS-NPs is employed as a strong material for dye decolourization and degradation application. Fig 7 (b) depicts linear relationship among $\ln(A_t/A_0)$ and time (min). For ZnS-NPs, the rate constant (k_{app}) value of the prepared ZnS-NPs 0.0024/min. The percentage degradation efficiency of ZnS-NPs for MB dye is plotted against irradiation time as represented in Fig 7(c). Here, the MB dye degraded maximum upto 93.24 %. The percent of degradation is scaled by equation % of Degradation= $[(A_0-A_t)/A_0] \times 100$. In which, A_0 implies dye absorbance at starting stage (zero min), A_t implies dye absorbance at time t. The photocatalytic studies of ZnS-NPs by related reviews are given in Table.1.

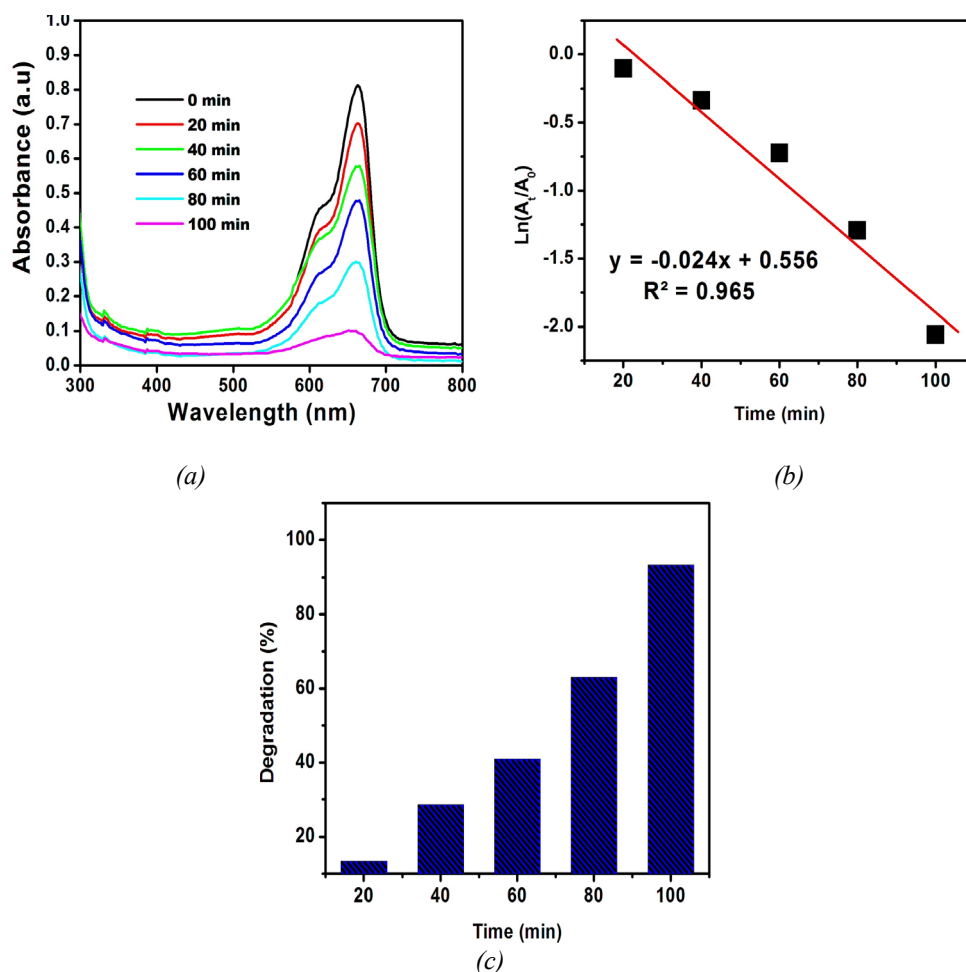


Fig. 7. (a) UV-Vis absorbance spectra, (b) absorption peak intensity ($\ln(A_t/A_0)$) plot and (c) a plot of percent of degradation efficiency of ZnS-NPs with time of degradation of MB dye.

Table 1. Related reviews Photocatalytic studies of ZnS-NPs.

S. No.	Materials	Source used	Dye used	Percentage of degradation (%)	Rate constant (K_{app}/min)	Time of irradiation (min)	reference
1	S/F/ZnS nanostructures	300 W lamp light	malachite green (MG)	74	0.0087	60	[57]
3	ZnS nanoparticles	visible light	MB	89.43	0.0015	240	[58]
4	ZnS microcrystal's	400 W high pressure mercury lamp	MB	91		60	[59]
5	ZnS spherical/flake nanostructures	UV-light radiation	Methyl Orange (MO)	51.7 and 84		150	[60]
6	ZnS nanoparticles	visible light	MB,	78.41	0.02052,	120	[61]
7	ZnS nanoparticles	UV light	MB	93.24	0.0024	100	Present study

3.7. Antibacterial studies of ZnS- nanoparticles

To examine the antibacterial actions of synthesized ZnS-NPs, the disc diffusion is used. Gram-negative, gram-positive, *E. Coli*, *S. aureus* considered as model test strains, which are commonly initiates in water. These involve the inoculating filter paper discs along synthesized ZnS-NPs, and then placed the discs in agar plate inoculated with specific organisms. The plate is inoculated at 35⁰ C for 24 hours. The vaccinated areas generated organism reticence zone, because it open out via the agar and indicated the antimicrobial movements. The inhibition area is calculated around the well with ZnS-NPs against the test organism. The biggest inhibition zone is measured against *E. coli* as 15.54 ± 0.031 mm and *S.aureus* had an inhibition zone of 7.32 ± 0.44, (Fig 8). The ZnS-NPs shows stronger inhibitory action against *E. coli*, Gram-positive bacteria, *S.aureus*. Due to differences in the typical characteristics such as structure and chemical composition of these two bacterial stains shows different inhibitory action (Fig.8). The cell wall of *S.aureus* has low amount of negative charged electrons as well as strong and denser peptidoglycan layer than *E. coli*. Gram-negative bacteria namely *E. coli* has superior penetrating power as well as good electrostatic interacting power with the nano sized particles in comparison with the positive charged bacteria. This results the higher inhibitory effect of *E. coli*. Vijayan et al, studied the antibacterial effect of ZnS-NPs [62]. The antibacterial efficiency of ZnS-NPs is depending on particle size, surface morphology, particular surface area and so on [63]. The antibacterial effect of ZnS-NPs is caused by electrostatic attraction amid the bacterial cell and ZnS nanoparticles. ZnS-NPs display a wide-spectrum biocide which is used to destroy, render harmless, or have some kind of controlling effect on a harmful organism towards multiple viruses, bacteria, and fungi [64-65].

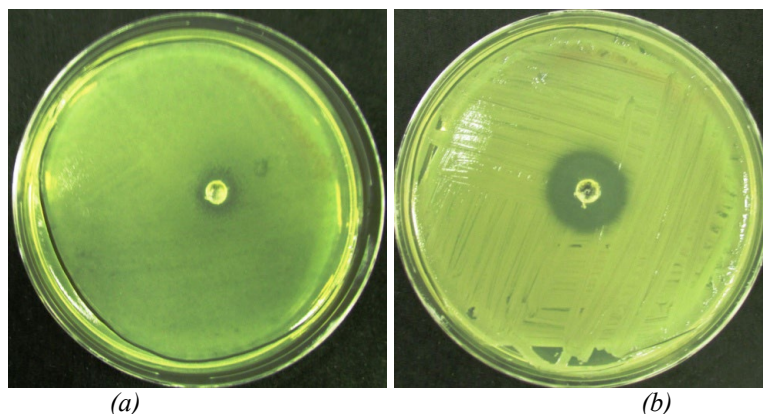


Fig. 8. The antibacterial activity of ZnS-NPs against (a) *S. aureus* and (b) *E. coli*.

4. Conclusion

In this study, ZnS-NPs is successfully synthesized by microwave enabled chemical precipitation method. According to structural analyses, the synthesized sample has a cubic structure. The ZnS-NPs shows phase transition above 450 K. Temperature resistance curve, the HT-XRDs at 373 K and 473 K and TG-DTA curve of ZnS-NPs clearly confirms the structural transition from cubic to hexagonal phase. The XRD patterns and temperature resistance curve clearly indicates that phase transition can be studied from temperature resistance measurements. The TGA and DTA outcomes prove that the incorporation of ZnS-NPs substantially altered the thermal properties displaying higher thermal stability. Absorption spectrum of the ZnS-NPs shows that there is an absorption band below 350 nm. Since ZnS-NPs emit light in the visible spectral range, this material can be used in the fabrication of optoelectronic devices. The Raman spectrum shows the transverse optical (TO) phonon mode around 290 cm^{-1} and the longitudinal optical mode (LO) around 340 cm^{-1} . The TEM image of cubic ZnS-NPs reveals the well distribution of spherical shaped ZnS-NPs. Photocatalytic studies clearly indicate that ZnS-NPs is employed as a strong material for dye decolourization and degradation application and water pollutants degradation of without any toxic by products. The synthesized ZnS nanoparticles displayed a pronounced antibacterial actions against various clinically pathogenic microorganisms.

References

- [1] M. Ghaedi, A. Asfaram, I. Tyagi, V. Kumar Gupta, S. Agarwal, RSC Adv. 2015 18438,18450; <https://doi.org/10.1039/C4RA15637D>
- [2] M. Guo, M. Song, S. Li, Z. Yin, X. Song, Y. Bu, CrystEngComm.2017. 2380,2393; <https://doi.org/10.1039/C7CE00360A>
- [3] M. Arif, Z. Min, L. Yuting, H. Yin, X. Liu, J. Ind. Eng. Chem. 2019, 345,357; <https://doi.org/10.1016/j.jiec.2018.09.026>
- [4] M. Arif, Q. Li, J. Yao, T. Huang, Y. Hua, T. Liu, X. Liu, J. Environ.Chem. Eng. 2017 .5358-5368; <https://doi.org/10.1016/j.jece.2017.10.024>
- [5] M. Arif, M. Zhang, J. Yao, H. Yin, P. Li, I. Hussain, X. Liu, J. AlloysCompd. 2019 ,878,893; <https://doi.org/10.1016/j.jallcom.2019.03.321>
- [6] M. Muruganandham, R. Amutha, E. Repo, M. Sillanpa, Y. Kusumoto, M. Abdulla-Al-Mamun, J. Photochem.Photobiol. Chem. 2010, 133,141; <https://doi.org/10.1016/j.jphotochem.2010.06.008>
- [7] M.E. Borges, M. Sierra, E. Cuevas, R.D. García, P. Esparza, Sol. Energy .2016, 527,535; <https://doi.org/10.1016/j.solener.2016.06.022>
- [8] M. Shahnas Beegam, S.G. Ullattil, P. Periyat Sol. Energy . 2018. 10,17;

<https://doi.org/10.1016/j.solener.2017.11.065>

- [9] Fang, X. Zhai, T. Gautam, U. K. Li, L. Wu, L. Bando, Y. Golberg, D. Prog. Mater. Sci. 2011, 56, 175; <https://doi.org/10.1016/j.pmatsci.2010.10.001>
- [10] Faze, W.; Maojun, Z.; Changqing, Z.; Bin, Z.; Wen, C.; Li, M.; Wenzhong, S. Nanotechnology 2015, 26, 345402; <https://doi.org/10.1088/0957-4484/26/34/345402>
- [11] Zhou, R.; Guzman, M. I. J. Phys. Chem. C 2014, 118, 11649; <https://doi.org/10.1021/jp4126039>
- [12] Jia, W. Jia, B. Qu, F. Wu, X. Dalton Trans. 2013, 42, 14178; <https://doi.org/10.1039/c3dt51712h>
- [13] Muruganandham, M.; Amutha, R.; Repo, E.; Sillanpää, M.; Kusumoto, Y.; Abdulla-Al-Mamun, M. J. Photochem. Photobiol. A 2010, 216, 133; <https://doi.org/10.1016/j.jphotochem.2010.06.008>
- [14] Chen, D. Huang, F. Ren, G. Li, D. Zheng, M. Wang, Y. Lin, Z. Nanoscale 2010, 2, 2062; <https://doi.org/10.1039/c0nr00171f>
- [15] Chauhan, Ruby; Kumar, Ashavani; Pal Chaudhary, Ram, Journal of Luminescence, 2014 6,12; <https://doi.org/10.1016/j.jlumin.2013.07.005>
- [16] Soltani, Nayereh, Saion, Elias, Mahmood Mat Yunus, W. Navasery, Manizheh; Bahmanrokh, Ghazaleh, Erfani, Maryam, Zare, Mohammad Reza, Gharibshahi, Elham, Solar Energy, 2013 147,154; <https://doi.org/10.1016/j.solener.2013.08.023>
- [17] Guo, Jing, Khan, Sovann, Cho, So-Hye; Kim, Jeonghwan r. Applied Surface Science, 425,432
- [18] Manoj Sharma , Tarun Jain , Sukhvir Singh , O.P. Pandey. Solar Energy, 2012 626,633.
- [19] Celikkaya, A.; Akinc, M. J. Am. Ceram. Soc. 1990, 73, 245; <https://doi.org/10.1111/j.1151-2916.1990.tb06501.x>
- [20] Li, X.; Hu, C.; Liu, H.; Xu, J.; Wan, B.; Wang, X. Physica E 2011, 43, 1071; <https://doi.org/10.1016/j.physe.2011.01.001>
- [21] Hu, J.-S.; Ren, L.-L.; Guo, Y.-G.; Liang, H.-P.; Cao, A.-M.; Wan, L.-J.; Bai, C.-L. Angew. Chem., Int. Ed. 2005, 44, 1269; <https://doi.org/10.1002/anie.200462057>
- [22] Fang, X. S.; Ye, C. H.; Zhang, L. D.; Wang, Y. H.; Wu, Y. C. Adv. Func. Mater. 2005, 15, 63; <https://doi.org/10.1002/adfm.200305008>
- [23] Hong, Y.; Lin, Z.; Huang, J.; Wang, Y.; Huang, F. Nanoscale 2011, 3, 1512; <https://doi.org/10.1039/c0nr00959h>
- [24] Linlin W, Chen H and Longquan S 2017 Int. J. Nanomed. 12 1227
- [25] Sathishkumar M, Saroja M, Venkatachalam M and Senthilkumar M 2016 Elixir Elec. Eng. 101 44118
- [26] Antibiotics Y C and Ozcengiz G 2017 Biochem. Pharmacol. 133 43
- [27] Rajapandiyan K, Jegan A, Vaiyapuri S P, Abdulraheem R A, Mohammed A A, Mustafa A G et al 2018 Microb. Pathogen. 120 85
- [28] Madalina E G, Elena R B, Alina M H, Monica C G and Alexandru M G 2016 Pharmaceuticals 9 75.
- [29] Felipe A. La Porta, Mateus M. Ferrer , Yuri V.B. Santana, Cristiane W. Raubach , Valéria M. Longo , Júlio R. Sambrano , Elson Longo , Juan Andrés , Máximo S. Li e , Jos A. Varela Journal of Alloys and Compounds 2013. 556,153,159; <https://doi.org/10.1016/j.jallcom.2012.12.081>
- [30] Tran Thi Quynh Hoa, Le Van Vu, Ta Dinh Canh and Nguyen Ngoc Long, Journal of Physics: Conference Series, 2009, 187, 012081; <https://doi.org/10.1088/1742-6596/187/1/012081>
- [31] Lellala Kashinath, Keerthiraj Namratha, Shivanna Srikantaswamy , Ajayan Vinu and Kullaiiah Byrappa ., New J. Chem., 2017, 41, 1723-1735; <https://doi.org/10.1039/C6NJ03716J>
- [32] J.R.Lij, huang, L. Cao, J, P. Wu H, Materials Science and Technology, 2010, 26(10), 1269-1272; <https://doi.org/10.1179/026708309X12495548508428>
- [33] Sakthivel, Thangavel, Karthikeyan Krishnamoorthy, Sang Jae Kim, Gunasekaran Venugopal. Journal of Alloys and Compounds, 2016; <https://doi.org/10.1016/j.jallcom.2016.05.089>
- [34] Tawatchai Charinpanitkul, Amornsak Chanagul, Joydeep Dutta, Uracha Rungsardthong

- ,Wiwut Tanthapanichakoon. Science and Technology of Advanced Materials 6 ,2005, 266,271;
<https://doi.org/10.1016/j.stam.2005.02.005>
- [35] S. B. Qadri, E. F. Skelton, D. Hsu, A. D. Dinsmore, J. Yang, H. F. Gray, and B. R. Ratna,Physical review B condensed matter and material physics.1999;
<https://doi.org/10.1103/PhysRevB.60.9191>
- [36]Cuizhuo Yang, Yanguo Liu , Hongyu Sun , Defeng Guo , Xiaohong Li , Wei Li , Baoting Liu , Xiangyi Zhang,2008 Nanotechnology, Volume 19, Number 9; <https://doi.org/10.1088/0957-4484/19/9/095704>
- [37] Arup Kanti Kole, Pathik Kumbhakar. Results in Physics 2,150,155
- [38] Yiyu Li, Wenxia Tan, and Yiquan Wu 2019,Manuscript
- [39]Do, Jeong Yeon; Choi, Suhwan; Nahm, Keehyung; Kim, Seog K.; Kang, Misook Materials Research Bulletin,2018 100, 234-242; <https://doi.org/10.1016/j.materresbull.2017.12.034>
- [40] M. AmalinSobi,D.Usha,M.Umadevi,M.R.Bindhu,ShanmugamSureshkumar,Munirah AbdullahAl-Dosary,Hissah AbdulrahmanAlodaini,Ashraf AtefHatamleh, Journal of King Saud University - Science,2022.34 , 102096; <https://doi.org/10.1016/j.jksus.2022.102096>
- [41] J. Kennedy , P.P. Murmu , P.S. Gupta , D.A. Carder , S.V. Chong , J. Leveneur , S. Rubanov. Materials Science in Semiconductor Processing.2014,26,561,566;
<https://doi.org/10.1016/j.mssp.2014.05.055>
- [42] Moly M. Rose, R. Sheela Christy, T. Asenath Benitta, J. Thampi Thanka Kumaran,2021,AIP Advances 11, 085129; <https://doi.org/10.1063/5.0052078>
- [43] Senapati U. S. Jha D.K. ,. Res. J. Chem. Sci. , 5(1), 33-40.
- [44]B. Sreenivasulu, S. Venkatramana Reddy, P. Venkateswara Reddy (2017)Synthesis and Properties of (Co, Ni) Co-Doped ZnSNanoparticles. Journal of Materials;
<https://doi.org/10.1007/s10854-017-7911-5>
- [45] S. A. Waly , M. M. Shehata , and H. H. Mahmoud (2017). Synthesis and Characterization of CdS Nanoparticles Prepared by Precipitation in the Presence of Span 20as Surfactant. Russian Journal of Applied Chemistry 90: 292–297; <https://doi.org/10.1134/S1070427217020203>
- [46] Ranjith Balu, Suresh Sagadevan, Arivuoli Dakshanamoorthy(2019) A Cost Effective, Facile Hydrothermal Approach of Zinc Sulfide Decorated on Graphene Nanocomposite forSupercapacitor Applications.Journal of Nanoscience and Nanotechnology Vol. 19, 6987-6994, 2019; <https://doi.org/10.1166/jnn.2019.16670>
- [47] Durand urdu M 2009 J. Phys. Chem. Solids 70 645;
<https://doi.org/10.1016/j.jpcs.2009.01.008>
- [48]D. Ayodhya, G. Veerabhadram, J. Inorg. Organomet. Polym. Mater.,2017, 27 , 215,230;
<https://doi.org/10.1007/s10904-017-0672-z>
- [49]R Boulkroune,M.Sebais, Y Messai, R Bourzami, M Schmutz, C Blanck,O Halimi, B Bull. Mater. Sci.2019 42,223; <https://doi.org/10.1007/s12034-019-1905-2>
- [50] S. Saravana Kumar , M. Abdul Khadar ,S.K. Dhara , T.R. Ravindran , K.G.M. Nair. Nuclear Instruments and Methods in Physics Research B 251, 435,440
- [51]Nada K.Abbas , Khalid, T. Al- Rasoul , Zainb J. Shanan . Int. J. Electrochem. Sci. 8 3049 - 3056
- [52] R. Mendil ,Z. Ben Ayadi , K. Djessas,2016, Journal of Alloys and Compounds 678, 87,92
<https://doi.org/10.1016/j.jallcom.2016.03.171>
- [53] Harish, G.S.; Sreedhara Reddy, P. (2015). Physica B: Condensed Matter, 473, 48,53;
<https://doi.org/10.1016/j.physb.2015.04.042>
- [54] O. Brafman, S.S. Mitra, Phys. Rev. 171 (1968) 931-934;
<https://doi.org/10.1103/PhysRev.171.931>
- [55] Meseguer, F. Colloids Surf., A 2005, 270, 1; <https://doi.org/10.1016/j.colsurfa.2005.05.038>
- [56] Collins, G, Armstrong, E, McNulty, D., O'Hanlon, S.; Geaney, H, O'Dwyer, C. Sci. Technol. Adv. Mater. 2016, 17, 563; <https://doi.org/10.1080/14686996.2016.1226121>
- [57] Shonisani Munyai, Louisa M Mahlaule-Glory and Noms, Charmaine Hintsho-Mbita, Mater.

- Res. Express 2022 9 , 015001; <https://doi.org/10.1088/2053-1591/ac4409>
- [58] Chen, Xiaobing; Li, He; Chen, Minfang; Li, Wenjiang; Yuan, Zhihao; Snyders, Rony 2019; <https://doi.org/10.1016/j.matchemphys.2019.01.055>
- [59] Zhang, Shuju 2014 Ceramics International, 40(3), 4553, 4557; <https://doi.org/10.1016/j.ceramint.2013.08.131>
- [60] Gajendiran, J.; Gnanam, S.; Vijaya Kumar, V.; Ramachandran, K.; Ramya, J. Chemical Physics Letters, Volume 754, article id. 137639; <https://doi.org/10.1016/j.cplett.2020.137639>
- [61] Ramana; Gokul Raj, S.; Sivakumar, N. Chemical Physics Letters, 754(), 137639; <https://doi.org/10.1016/j.cplett.2020.137639>
- [62] Vijayan, S., Dash, C. S., Umadevi, G., Sundararajan, M., & Mariappan, R. (2020). Investigation of Structural, Optical and Antibacterial Activity of ZnS Nanoparticles. Journal of Cluster Science; <https://doi.org/10.1007/s10876-020-01923-3>
- [63] S Jesudoss, J. J. Vijaya, L. J. Kennedy, P. I. Rajan, H. A. Al-Lohedan, R. J. R. K. Amalingam, and M. Bououdina (2016). J. Photochem. Photobiol. B. Biol. 165, 121-132; <https://doi.org/10.1016/j.jphotobiol.2016.10.004>
- [64] Jin, S.-E.; Jin, H.-E. Antimicrobial Activity of Zinc Oxide Nano/Microparticles and Their Combinations against Pathogenic Microorganisms for Biomedical Applications: From Physicochemical Characteristics to Pharmacological Aspects. Nanomaterials 2021, 11; <https://doi.org/10.3390/nano11020263>
- [65] Liu, Y.; Huang, J.; Feng, X.; Li, H. Thermal-Sprayed Photocatalytic Coatings for Biocidal Applications: A Review. J. Therm. Spray Technol. 2020